2023 IEEE International Conference on Robotics and Automation (ICRA 2023)
May 29 - June 2, 2023. London, UK

QuadMag: A Mobile-Coil System With Enhanced Magnetic Actuation Efficiency and Dexterity

Lidong Yang, Moqiu Zhang, Zhengxin Yang, Haojin Yang, and Li Zhang

Abstract— **Magnetic field is a favorable power source for actuation and control of micro-/nanorobots. To overcome the fast decay of magnetic field for large-workspace microrobotic actuation, mobile field source-based systems have been proposed. In this work, we report a new mobile-coil system, i.e., QuadMag. It consists of four electromagnetic coils, whose motion is actuated by a parallel mechanism. Compared to previous systems with three mobile coils, e.g., DeltaMag, the additional coil in the QuadMag increases the degree-of-freedom (DoF) for magnetic control. However, to control QuadMag, new control methods should be developed for the over-constrained parallel mechanism and for the field/force of the four coils. We derive the Jacobian matrix for the differential motion of the parallel mechanism and then formulate the field, force and simultaneous field and force control methods for magnetic actuation. Comparative experiments validate the enhanced actuation efficiency when controlling torque-driven helical microrobots. Moreover, the magnetic actuation dexterity is also enhanced by the additional coil. We conduct simulated navigation experiments and prove the actuation capability of QuadMag for 3D force-driven microrobot navigation with controlled robot orientation.**

I. Introduction

The microrobotics field has been developing very fast in recent years [1]–[4]. Regarding the power sources for wireless microrobot actuation, magnetic field is the most favorable one due to its high controllability and biocompatibility. Also, its penetration ability to biological tissues makes magnetic microrobots good candidates for biomedicine. Recently, studies on magnetic microrobots have paved the way to real applications [5]–[12]. From the robotics perspective, motion control of magnetic microrobots is the foundation of such applications [13], and related techniques have provided solutions to individual [14], multiple [15], [16], and swarm [17]–[20] microrobot control. These techniques endow magnetic microrobots with the efficient and automated navigation capability for targeted delivery/therapy.

This work was supported by the Hong Kong RGC with project Nos. 14300621, E-CUHK401/20, and RFS2122-4S03; the RGC/RFS project No. RFS2122-4S03, the RGC/RIF project No. R4015-21; the Croucher Foundation Grant with Ref. No. CAS20403; and the CUHK internal grants. We thank the support from Multi-scale Medical Robotics Center (MRC), InnoHK, at the Hong Kong Science Park, and the SIAT-CUHK Joint Laboratory of Robotics and Intelligent Systems. (e-mail: lidong.yang@polyu.edu.hk; lizhang@mae.cuhk.edu.hk)

L. Yang is with The Department of Industrial and Systems Engineering, The Hong Kong Polytechnic University (PolyU), Kowloon, Hong Kong, China.

M. Zhang, Z. Yang, H. Yang and L. Zhang are with The Department of Mechanical and Automation Engineering, The Chinese University of Hong Kong (CUHK), Shatin NT, Hong Kong, China.

L. Zhang is also with The CUHK T Stone Robotics Institute and The Chow Yuk Ho Technology Centre for Innovative Medicine, The Chinese University of Hong Kong (CUHK), Shatin NT, Hong Kong, China.

The untethered control manner of magnetic microrobots require an external magnetic actuation system to generate controllable magnetic fields [21]. Such systems can be classified into two categories: permanent magnet-based and electromagnetic coil-based. As the field of a magnet is constant, the pose of the magnet should be changed by robot arms [22] or motors [23] to generate dynamic magnetic fields. The limited bandwidth of the mechanical motion may put constraints on the allowable field frequency. This type of system has recently witnessed the advances in active in-body catheter manipulation [24]. In comparison, the field of coil-based systems can be easily controlled by regulating the coil currents. Various system configurations composed of arrays of stationary coils have been designed that are capable of high-frequency microrobotic actuation, for example the Helmholtz system [25], the OctoMag system [26], and many others [27], [28]. To strengthen the produced magnetic fields, coils are usually wrapped on iron cores, resulting in more complex system structures (e.g., the cooling module) and larger system volumes than those of the permanent magnet-based systems. Thus, to provide human-body-scale workspace, the fast decay of magnetic field would result in bulky coil-based systems, such as the CardioMag system [29] and the Aeon Phocus system [30]. In addition, the large coil would exhibit high inductance and power consumption.

Mobile coil-based systems, first introduced in [31], provide an alternative design for large-workspace microrobotic actuation. Coils are manipulated by robotic mechanisms to reach desired poses, and coil currents are simultaneously controlled to generate desired magnetic fields [32]. However, development of such systems containing multiple coils is challenging. Firstly, the large sizes/weights of coils require sophisticated mechanism design to actuate the coils' motion. Secondly, owing to the nonlinear and non-intuitive field distribution of an electromagnetic coil, position and pose variations of multiple coils lead to challenges in real-time computation of the resulting composite field as well as the inverse computation problem of coil poses and currents. Recently, the DeltaMag [33] and RoboMag [34] are proposed, in which the motion of three coils are actuated by the parallel mechanism and robotic arms, respectively. However, how to extend the system design and control to more than three coils is untackled, which is necessary to increase the field control DoF so as to enhance the system capabilities in terms of magnetic actuation efficiency and dexterity.

In this paper, we propose the QuadMag system that consists of four mobile coils whose motion is actuated by an over-constrained parallel mechanism. As shown in Fig.

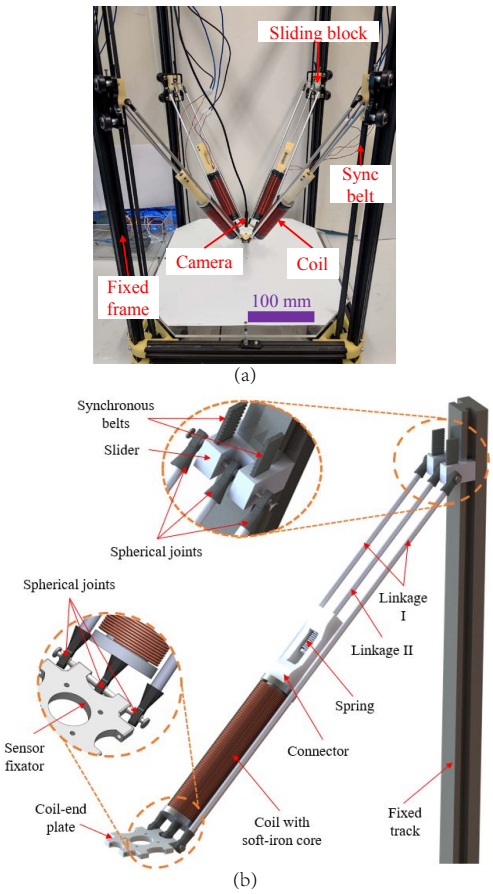

Fig. 1. The mechanical part of QuadMag. (b) A photo of the QuadMag mechanism. (b) The mechanical design of each branch of QuadMag.

1(a), the system structure makes the four coils integrated into the parallel branches. By this design, the coil volumes do not interfere with the workspace of the parallel mechanism. In addition, every coil in the system has non-overlapping motion with the other ones, ensuring the intrinsic safe mechanical motion. Unlike DeltaMag, the parallel mechanism in QuadMag becomes over-constrained, i.e., eight points constraints on the coil-end plate. As a result, the inverse kinematics-based position control used in DeltaMag [33] would lose effectiveness. In addition to the difference in mechanical motion control, the extra coil increases the DoF of magnetic control. We have applied DeltaMag for controlling catheter [35] and microrobots [36], for which, to generate a 3D field, the coil currents have unique solutions. Since QuadMag contains four coils, it has redundancy for the 3D field generation that can be utilized for other control purposes, e.g., optimization of the coil currents. Furthermore, the increase of the magnetic control DoF makes it possible to perform the simultaneous magnetic field and force control, which is beyond the capability of the DeltaMag system.

II. System Overview of QuadMag

The QuadMag system mainly consists of four components: the mechanical part, the mechanical motion control module, the coil current control module, and the host computer for high-level task computation.

Mechanical part: Fig. 1(b) illustrates the mechanical design of one coil branch of QuadMag. Each coil is integrated into the parallel mechanism by two spherical joints. To tolerate fabrication error, the Linkage II and a spring is adopted to connect the coil and the sliding block. The sliding block moving on a vertically fixed linear track is driven by a synchronous belt. The other ends of the four branches are attached to the 'coil-end plate'. By this design, each coil moves with the parallelogram mechanism, and pose/position of the coil can be deduced via mathematical formulation. This parallel mechanism can drive the coil-end plate to a cylindrical workspace of $\Phi 200 \times 300$ mm^3. Regarding the state feedback, cameras can be installed on the coil-end plate, and such eye-in-hand configuration enables the large-workspace and high-resolution microrobot tracking.

Mechanical motion control module: A stepper motor drives the synchronous belt for the motion of the sliding block. To realize correct mechanical motion, the four motors are simultaneously controlled by an Arduino Mega 2560 with a control frequency of 100 Hz. Desired positions of the coil-end plate are planned by the host computer and then sent to the Arduino via serial communication (50 Hz). Mechanical motion control method formulated in the next section is implemented in the Arduino. After it receives the next position of the coil-end plate, the Arduino executes the control method and makes the four motors output correct actions. At the same time, the Arduino also transmits the current positions of the four sliding blocks to the host computer which is required in the magnetic field control.

Coil current control module: Each of the four coils is driven by a servo-amplifier (Model: ESCON 70/10, Maxon Inc.), and the maximum output current is 10 A. Coils are equipped with 1J22 soft iron cores to strengthen the field. It is measured that the maximum field is 23 mT at the axial distance of 30 mm. The host computer sends desired coil currents to servo-amplifiers via a multifunctional I/O card (Model: 826, Sensoray Inc.), and then the servo-amplifiers output the required currents in the four coils.

Host computer: Computation of the high-level tasks are accomplished by the host computer, which mainly include: (1) image processing to obtain the current position of the working microrobot; (2) planning of the motion of the coil-end plate and transmitting it to the Arduino; (3) calculation of the desired magnetic field/force according to the control task; (4) calculation of the required coil currents of the four coils and transmitting them to the servo-amplifiers.

III. Mechanical Motion Control

A. Mechanism constraints of QuadMag

The geometric representation of the k-th ($k \in \{1, 2, 3, 4\}$) branch of QuadMag is depicted as Fig. 2, in which vectors (e.g., $\hat{\mathbf{n}}_{\mathrm{P}}^{\mathcal{G}}$) are denoted by lower-case bold font, and the superscript and subscript are their coordinate frame and identifier, respectively. The 'hat' symbol marks unit vectors. Space points are marked by upper-case standard font, for

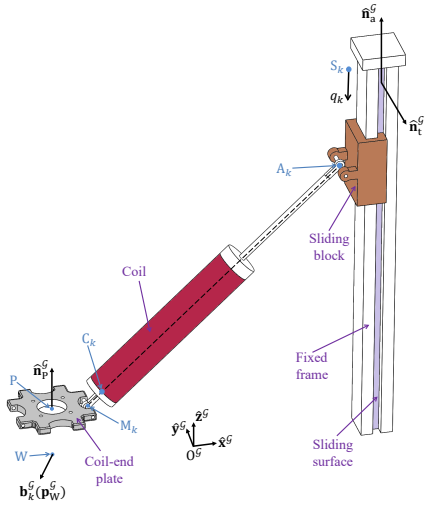

Fig. 2. Geometric representation of k-th branch of the QuadMag. Important points and vectors for kinematics modelling and field computation are marked in the figure. $\mathbf{b}_k^{\mathcal{G}}(\mathbf{p}_{\mathrm{W}}^{\mathcal{G}}) \in \mathbb{R}^3$ denotes the field vector of the k-th coil at point W.

example, points P and W denote the positions of the coil-end plate center and the working point where the magnetic microrobotic device locates, respectively. Variables and constants are marked by lower-case and upper-case italic fonts, respectively.

The four coil branches are uniformly distributed around $\hat{\mathbf{n}}_{\mathrm{P}}^{\mathcal{G}}$ (the normal vector of the coil-end plate). To make sure the coil branches can be well attached on the coil-end plate without physical interference among them, the distance between point P and point M_k should be large enough. This design makes each coil branch provide two point constraints on the coil-end plate. That is, three branches (i.e., six point constraints) is sufficient to fully constrain the coil-end plate motion, as shown in the DeltaMag system. Although this fact, it would be necessary to adopt more coils to increase the DOFs of the magnetic control [37]. The QuadMag extends the magnetic control DoF to four, and combining its motion control DoFs, it has the capability of simultaneous field and force magnetic control. However, on the other side, the coil-end plate is over-constrained by eight points of the four branches that leads to the difficulty of the mechanical motion control.

B. Differential Control Method

To make the over-constrained parallel mechanism work correctly, the eight point constraints should be satisfied at any time instants. For this objective, the inverse kinematics-based method for DeltaMag is infeasible, and we propose the differential motion-based method. That is, velocities of all the four actuators are precisely controlled in real time.

Referring Fig. 2, the coordinate of M_k at the global coordinate frame $\{\mathcal{G} : \mathrm{O}^{\mathcal{G}} - \hat{x}^{\mathcal{G}}\hat{y}^{\mathcal{G}}\hat{z}^{\mathcal{G}}\}$ can be obtained by

$$\mathbf{p}_{\mathrm{M}_k}^{\mathcal{G}} = \begin{bmatrix} x_{\mathrm{M}_k} \\ y_{\mathrm{M}_k} \\ z_{\mathrm{M}_k} \end{bmatrix} = \begin{bmatrix} x_{\mathrm{P}} + L_{\mathrm{MP}} \cos\alpha_k \\ y_{\mathrm{P}} + L_{\mathrm{MP}} \sin\alpha_k \\ z_{\mathrm{P}} \end{bmatrix} \tag{1}$$

where L_{MP} is a constant length between point P and point M_k. $\mathbf{p}_{\mathrm{P}}^{\mathcal{G}} = [x_{\mathrm{P}}\ y_{\mathrm{P}}\ z_{\mathrm{P}}]^{\mathrm{T}} \in \mathbb{R}^3$ represents the coordinate of the coil-end plate center and α_k is defined as

$$\alpha_k = 90^\circ \times (k-1), \quad k = 1, 2, 3, 4 \tag{2}$$

The coordinate of A_k is calculated by

$$\mathbf{p}_{\mathrm{A}_k}^{\mathcal{G}} = \begin{bmatrix} x_{\mathrm{A}_k} \\ y_{\mathrm{A}_k} \\ z_{\mathrm{A}_k} \end{bmatrix} = \begin{bmatrix} L_{\mathrm{h}} \cos\alpha_k \\ L_{\mathrm{h}} \sin\alpha_k \\ L_{\mathrm{v}} - q_k \end{bmatrix} \tag{3}$$

where L_{h} and L_{v} are the constant horizontal and vertical distances between $\mathrm{O}^{\mathcal{G}}$ and A_k respectively. q_k is the position of the k-th sliding block starting from point S_k. Due to the parallelogram structure, $||\mathbf{p}_{\mathrm{A}_k}^{\mathcal{G}} - \mathbf{p}_{\mathrm{M}_k}^{\mathcal{G}}||$ is a constant, that is

$$||\mathbf{p}_{\mathrm{A}_k}^{\mathcal{G}} - \mathbf{p}_{\mathrm{M}_k}^{\mathcal{G}}|| - L_{\mathrm{AM}} = 0 \tag{4}$$

where L_{AM} is a constant length between point A_k and M_k.

Substitute Eq. (1) and (3) into (4), then we have

$$(x_{\mathrm{P}} - x_k)^2 + (y_{\mathrm{P}} - y_k)^2 + (z_{\mathrm{P}} - z_k)^2 = L_{\mathrm{AM}}^2 \tag{5}$$

in which

$$\begin{cases} x_k = L_{\mathrm{h}} \cos\alpha_k - L_{\mathrm{MP}} \cos\alpha_k \\ y_k = L_{\mathrm{h}} \sin\alpha_k - L_{\mathrm{MP}} \sin\alpha_k \\ z_k = L_{\mathrm{v}} - q_k \end{cases} \tag{6}$$

Differentiating Eq. (5) with respect to time leads to

$$(x_{\mathrm{P}} - x_k)\dot{x}_{\mathrm{P}} + (x_{\mathrm{P}} - y_k)\dot{y}_{\mathrm{P}} + (z_{\mathrm{P}} - x_k)\dot{z}_{\mathrm{P}} = \frac{\dot{q}_k}{z_k - z_{\mathrm{P}}} \tag{7}$$

Rearrange Eq. (7), then we have

$$\dot{\mathbf{q}} = \mathbf{J}_{\mathrm{m}} \dot{\mathbf{p}}_{\mathrm{P}}^{\mathcal{G}} \tag{8}$$

where $\mathbf{q} = [q_1\ q_2\ q_3\ q_4]^{\mathrm{T}}$. Thus, $\mathbf{J}_{\mathrm{m}}$ is the Jacobian matrix that relates the velocity of the coil-end plate to the velocities of the sliding blocks, which has the following expression:

$$\mathbf{J}_{\mathrm{m}} = \begin{bmatrix} \frac{x_{\mathrm{P}} - x_1}{z_1 - z_{\mathrm{P}}} & \frac{y_{\mathrm{P}} - y_1}{z_1 - z_{\mathrm{P}}} & -1 \\ \frac{x_{\mathrm{P}} - x_2}{z_2 - z_{\mathrm{P}}} & \frac{y_{\mathrm{P}} - y_2}{z_2 - z_{\mathrm{P}}} & -1 \\ \frac{x_{\mathrm{P}} - x_3}{z_3 - z_{\mathrm{P}}} & \frac{y_{\mathrm{P}} - y_3}{z_3 - z_{\mathrm{P}}} & -1 \\ \frac{x_{\mathrm{P}} - x_4}{z_4 - z_{\mathrm{P}}} & \frac{y_{\mathrm{P}} - y_4}{z_4 - z_{\mathrm{P}}} & -1 \end{bmatrix} \tag{9}$$

Using Eq. (8), the mechanical motion of QuadMag can be controlled in a differential manner to fulfill the mechanical constraints. $\mathbf{p}_{\mathrm{P}}^{\mathcal{G}}$ and $\mathbf{q}$ at time instant $N\Delta t$ can be obtained by

$$\begin{cases} \mathbf{p}_{\mathrm{P}}^{\mathcal{G}}(N\Delta t) = \sum_{n=0}^{N} \left\{ \dot{\mathbf{p}}_{\mathrm{P}}^{\mathcal{G}}(n\Delta t) \cdot \Delta t \right\} \\ \mathbf{q}(N\Delta t) = \sum_{n=0}^{N} \left\{ \mathbf{J}_{\mathrm{m}}(n\Delta t) \dot{\mathbf{p}}_{\mathrm{P}}^{\mathcal{G}}(n\Delta t) \cdot \Delta t \right\} \end{cases} \tag{10}$$

where Δt denotes the control interval of the Arduino.

IV. Magnetic Field and Force Control

When actuating microrobots in large space, poses of the four coils should be adjusted in pace with the microrobot. Therefore, magnetic control inputs should be recalculated which is not straight-forward due to the non-intuitive field distribution around the coils. This section will present how to control the field and force of QuadMag as well as their simultaneous control.

A. Magnetic Field Control

To compute the composite field of the four coils, we first transform $\mathbf{p}_{\mathrm{W}}^{\mathcal{G}}$, i.e., the position of the microrobot, to the coils' local frames $\{\mathcal{C}_k : \mathrm{O}^{\mathcal{C}_k} - \hat{\mathbf{x}}^{\mathcal{C}_k}\hat{\mathbf{y}}^{\mathcal{C}_k}\hat{\mathbf{z}}^{\mathcal{C}_k}, k = 1, 2, 3, 4\}$. In the global frame, for the k-th coil, the origin $\mathrm{O}^{\mathcal{C}_k}$ of its local frame coincides with point C_k as shown in Fig. 2. The coordinate of C_k is computed by

$$\mathbf{p}_{\mathrm{C}_k}^{\mathcal{G}} = \begin{bmatrix} x_{\mathrm{C}_k} \\ y_{\mathrm{C}_k} \\ z_{\mathrm{C}_k} \end{bmatrix} = \mathbf{p}_{\mathrm{A}_k}^{\mathcal{G}} + \frac{L_{\mathrm{AC}}}{L_{\mathrm{AM}}}\left(\mathbf{p}_{\mathrm{M}_k}^{\mathcal{G}} - \mathbf{p}_{\mathrm{A}_k}^{\mathcal{G}}\right) \tag{11}$$

where L_{AC} is the constant length between A_k and C_k. Let $\mathbf{p}_{\mathrm{AC}_k}^{\mathcal{G}}$ denotes the vector from point A_k to point C_k, i.e., $\mathbf{p}_{\mathrm{AC}_k}^{\mathcal{G}} = \mathbf{p}_{\mathrm{C}_k}^{\mathcal{G}} - \mathbf{p}_{\mathrm{A}_k}^{\mathcal{G}}$, then, due to the cylindrical shape of the coil, vectors $\mathbf{p}_{\mathrm{AC}_k}^{\mathcal{G}}$, $\mathbf{p}_{\mathrm{CW}_k}^{\mathcal{G}}$ and the field vector $\bar{\mathbf{b}}_k^{\mathcal{G}}(\mathbf{p}_{\mathrm{W}}^{\mathcal{G}})$ are coplanar, the following function holds

$$\left| \begin{array}{ccc} \mathbf{p}_{\mathrm{AC}_k}^{\mathcal{G}} & \mathbf{p}_{\mathrm{CW}_k}^{\mathcal{G}} & \mathbf{b}_k^{\mathcal{G}}(\mathbf{p}_{\mathrm{W}}^{\mathcal{G}}) \end{array} \right| = 0 \tag{12}$$

where $\mathbf{p}_{\mathrm{CW}_k}^{\mathcal{G}}$ is defined by the same way as $\mathbf{p}_{\mathrm{AC}_k}^{\mathcal{G}}$, and $|\bullet|$ stands for the determinant operation. To simplify the computation, the local frame $\{\mathcal{C}_k\}$ is uniquely determined by three conditions: (1) its $\hat{\mathbf{z}}^{\mathcal{C}_k}$ direction aligns with the axial direction of the coil; (2) its $\hat{\mathbf{x}}^{\mathcal{C}_k}\hat{\mathbf{z}}^{\mathcal{C}_k}$ plane coincides with the plane expanded by the three vectors in Eq. (12); (3) its $\hat{\mathbf{x}}^{\mathcal{C}_k}$ direction is chosen such that $x_{\mathrm{W}}^{\mathcal{C}_k}$ is always greater than or equal to 0. Based on the three conditions, in the local frame of the k-th coil, the coordinates of W read

$$\begin{cases} z_{\mathrm{W}}^{\mathcal{C}_k} = \frac{\left(\mathbf{p}_{\mathrm{AC}_k}^{\mathcal{G}}\right)^{\mathrm{T}} \cdot \mathbf{p}_{\mathrm{CW}_k}^{\mathcal{G}}}{||\mathbf{p}_{\mathrm{AC}_k}^{\mathcal{G}}||} \\ y_{\mathrm{W}}^{\mathcal{C}_k} = 0 \\ x_{\mathrm{W}}^{\mathcal{C}_k} = \sqrt{||\mathbf{p}_{\mathrm{CW}_k}^{\mathcal{G}}||^2 - (z_{\mathrm{W}}^{\mathcal{C}_k})^2} \end{cases} \tag{13}$$

Now, the coordinates of W are transformed to the local frames of every coil. Assume the k-th coil with soft iron core is operated at its linear range, its magnetic flux density–$\mathbf{b}_k^{\mathcal{C}_k}$ (unit: mT) at $\mathbf{p}_{\mathrm{W}}^{\mathcal{C}_k}$ depends linearly on the coil current–i_k, which can be calculated by

$$\mathbf{b}_k^{\mathcal{C}_k}(\mathbf{p}_{\mathrm{W}}^{\mathcal{C}_k}) = i_k \cdot \bar{\mathbf{b}}_k^{\mathcal{C}_k}(\mathbf{p}_{\mathrm{W}}^{\mathcal{C}_k}) = i_k \cdot \overline{\mathcal{M}}_k^{\mathcal{C}_k}(\mathbf{p}_{\mathrm{W}}^{\mathcal{C}_k}) \tag{14}$$

where $\overline{\mathcal{M}}_k^{\mathcal{C}_k}(\bullet)$ stands for the unit field map of the k-th coil [33]. The overbar symbol marks unit field parameters that are induced by 1 A coil current.

After coordinate rotation transformation, the magnetic fields of the four coils in the global frame are obtained by

$$\mathbf{b}_k^{\mathcal{G}}(\mathbf{p}_{\mathrm{W}}^{\mathcal{G}}) = {}^{\mathcal{G}}\mathbf{R}_{\mathcal{C}_k}(\mathbf{p}_{\mathrm{W}}^{\mathcal{C}_k}, \mathbf{p}_{\mathrm{P}}^{\mathcal{G}}) \cdot \mathbf{b}_k^{\mathcal{C}_k}(\mathbf{p}_{\mathrm{W}}^{\mathcal{C}_k}) \tag{15}$$

where ${}^{\mathcal{G}}\mathbf{R}_{\mathcal{C}_k}(\mathbf{p}_{\mathrm{W}}^{\mathcal{C}_k}, \mathbf{p}_{\mathrm{P}}^{\mathcal{G}}) \in \mathbb{R}^{3\times3}$ is the corresponding rotation matrix with transformation from $\{\mathcal{C}_k\}$ to $\{\mathcal{G}\}$. According to the superposition property of magnetic fields, the total field at $\mathbf{p}_{\mathrm{W}}^{\mathcal{G}}$ can be calculated by

$$\mathbf{b}^{\mathcal{G}}(\mathbf{p}_{\mathrm{W}}^{\mathcal{G}}) = [\bar{\mathbf{b}}_1^{\mathcal{G}}(\mathbf{p}_{\mathrm{W}}^{\mathcal{G}})\ \bar{\mathbf{b}}_2^{\mathcal{G}}(\mathbf{p}_{\mathrm{W}}^{\mathcal{G}})\ \cdots\ \bar{\mathbf{b}}_4^{\mathcal{G}}(\mathbf{p}_{\mathrm{W}}^{\mathcal{G}})] \cdot \mathbf{i} = \bar{\mathbf{B}} \cdot \mathbf{i} \tag{16}$$

where $\mathbf{i} = [i_1\ i_2\ i_3\ i_4]^{\mathrm{T}}$ is the vector of coil currents.

If a desired field is given, the exact required coil currents can be obtained by

$$\mathbf{i} = \bar{\mathbf{B}}^{\dagger} \cdot \mathbf{b}^{\mathcal{G}}(\mathbf{p}_{\mathrm{W}}^{\mathcal{G}}) \tag{17}$$

where $\bar{\mathbf{B}}^{\dagger}$ represents the pseudo-inverse of $\bar{\mathbf{B}}$.

B. Magnetic Force Control

The magnetic force exerted on the microrobot depends on the gradient matrices of the four coils. Due to the cylindrical shape of the coil and the definition of the local frames, the unit gradient matrix of the k-th coil at $\mathbf{p}_{\mathrm{W}}^{\mathcal{C}_k}$ is simplified as

$$\bar{\mathbf{G}}_k^{\mathcal{C}_k}(\mathbf{p}_{\mathrm{W}}^{\mathcal{C}_k}) = \begin{bmatrix} \frac{\partial \overline{\mathcal{M}}_x(\mathbf{p}_{\mathrm{W}}^{\mathcal{C}_k})}{\partial x^{\mathcal{C}_k}} & 0 & \frac{\partial \overline{\mathcal{M}}_x(\mathbf{p}_{\mathrm{W}}^{\mathcal{C}_k})}{\partial z^{\mathcal{C}_k}} \\ 0 & \frac{\partial \overline{\mathcal{M}}_y(\mathbf{p}_{\mathrm{W}}^{\mathcal{C}_k})}{\partial y^{\mathcal{C}_k}} & 0 \\ \frac{\partial \overline{\mathcal{M}}_x(\mathbf{p}_{\mathrm{W}}^{\mathcal{C}_k})}{\partial z^{\mathcal{C}_k}} & 0 & \frac{\partial \overline{\mathcal{M}}_z(\mathbf{p}_{\mathrm{W}}^{\mathcal{C}_k})}{\partial z^{\mathcal{C}_k}} \end{bmatrix} \tag{18}$$

where $\frac{\partial \overline{\mathcal{M}}_z(\mathbf{p}_{\mathrm{W}}^{\mathcal{C}_k})}{\partial z^{\mathcal{C}_k}} = -\left(\frac{\partial \overline{\mathcal{M}}_y(\mathbf{p}_{\mathrm{W}}^{\mathcal{C}_k})}{\partial y^{\mathcal{C}_k}} + \frac{\partial \overline{\mathcal{M}}_x(\mathbf{p}_{\mathrm{W}}^{\mathcal{C}_k})}{\partial x^{\mathcal{C}_k}}\right)$. $\overline{\mathcal{M}}_x(\mathbf{p}_{\mathrm{W}}^{\mathcal{C}_k})$ represents the x component of the unit field map at $\mathbf{p}_{\mathrm{W}}^{\mathcal{C}_k}$.

To compute the composite magnetic force at the global frame, we need to first calculate the magnetic forces of the four coils at the coils' local frames considering that the gradient matrix is non-rotational. This step is expressed by

$$\begin{aligned} \tilde{\mathbf{f}}_k^{\mathcal{C}_k}(\mathbf{p}_{\mathrm{W}}^{\mathcal{C}_k}) &= \bar{\mathbf{G}}_k^{\mathcal{C}_k}(\mathbf{p}_{\mathrm{W}}^{\mathcal{C}_k}) \cdot \mathbf{m}^{\mathcal{C}_k} \\ &= \bar{\mathbf{G}}_k^{\mathcal{C}_k}(\mathbf{p}_{\mathrm{W}}^{\mathcal{C}_k}) \cdot {}^{\mathcal{C}_k}\mathbf{R}_{\mathcal{G}}(\mathbf{p}_{\mathrm{W}}^{\mathcal{G}}, \mathbf{p}_{\mathrm{P}}^{\mathcal{G}}) \cdot \mathbf{m}^{\mathcal{G}} \end{aligned} \tag{19}$$

where $\mathbf{m}^{\mathcal{G}}$ is the magnetic moment vector of the microrobot and ${}^{\mathcal{C}_k}\mathbf{R}_{\mathcal{G}}(\mathbf{p}_{\mathrm{W}}^{\mathcal{G}}, \mathbf{p}_{\mathrm{P}}^{\mathcal{G}}) = {}^{\mathcal{G}}\mathbf{R}_{\mathcal{C}_k}^{-1}(\mathbf{p}_{\mathrm{W}}^{\mathcal{C}_k}, \mathbf{p}_{\mathrm{P}}^{\mathcal{G}})$. Then, the unit magnetic forces are transformed to the global coordinate frame:

$$\tilde{\mathbf{f}}_k^{\mathcal{G}}(\mathbf{p}_{\mathrm{W}}^{\mathcal{G}}) = {}^{\mathcal{G}}\mathbf{R}_{\mathcal{C}_k}(\mathbf{p}_{\mathrm{W}}^{\mathcal{C}_k}, \mathbf{p}_{\mathrm{P}}^{\mathcal{G}}) \cdot \tilde{\mathbf{f}}_k^{\mathcal{C}_k}(\mathbf{p}_{\mathrm{W}}^{\mathcal{C}_k}, \mathbf{m}^{\mathcal{G}}) \tag{20}$$

According to the superposition principle, the total magnetic force at the microrobot location $\mathbf{p}_{\mathrm{W}}^{\mathcal{G}}$ can be calculated by

$$\mathbf{f}^{\mathcal{G}}(\mathbf{p}_{\mathrm{W}}^{\mathcal{G}}) = [\tilde{\mathbf{f}}_1^{\mathcal{G}}(\mathbf{p}_{\mathrm{W}}^{\mathcal{G}}, \mathbf{m}^{\mathcal{G}}) \cdots \tilde{\mathbf{f}}_4^{\mathcal{G}}(\mathbf{p}_{\mathrm{W}}^{\mathcal{G}}, \mathbf{m}^{\mathcal{G}})] \cdot \mathbf{i} = \bar{\mathbf{F}} \cdot \mathbf{i} \tag{21}$$

If the orientation of the microrobot is constrained by the working environment, i.e., $\mathbf{m}^{\mathcal{G}}$ does not change with the magnetic field, the required coil currents can be obtained by

$$\mathbf{i} = \bar{\mathbf{F}}^{\dagger} \cdot \mathbf{f}^{\mathcal{G}}(\mathbf{p}_{\mathrm{W}}^{\mathcal{G}}) \tag{22}$$

C. Simultaneous Field and Force Control

At some scenarios, the microrobot moves in free fluid and its orientation is required to be controlled, e.g., the endoscope [22]. For such applications, the magnetic field and force should be simultaneously controlled [26]. The additional magnetic control DoF and the mechanical motion DoFs make it possible to realize this objective.

In quasi-static magnetic manipulation, it is reasonable to assume that the magnetic moment of the robot aligns with the magnetic field, i.e.

$$\hat{\mathbf{b}}^{\mathcal{G}}(\mathbf{p}_{\mathrm{W}}^{\mathcal{G}}) = \hat{\mathbf{m}}^{\mathcal{G}} \tag{23}$$

Thus, we can achieve the required robot orientation by

$$\mathbf{i}' = \bar{\mathbf{B}}^{\dagger} \cdot \hat{\mathbf{m}}^{\mathcal{G}} \tag{24}$$

Then, we find the null space of $\bar{\mathbf{B}}$, i.e., $\mathbf{i}'' \in \mathbb{R}^3$, by solving

$$\bar{\mathbf{B}} \cdot \mathbf{i}'' = \mathbf{0} \tag{25}$$

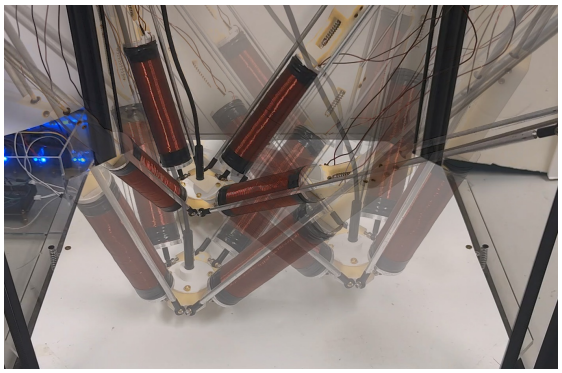

Fig. 3. Control of the mechanical motion of QuadMag in the workspace (diameter: 200 mm), which validates the control method and the constructed system. The control process is included in the Supporting video.

The magnetic force vectors corresponding to $\hat{\mathbf{i}}'$ and $\hat{\mathbf{i}}''$ are

$$\begin{cases} \tilde{\mathbf{f}}' = \bar{\mathbf{F}} \cdot \hat{\mathbf{i}}' \\ \tilde{\mathbf{f}}'' = \bar{\mathbf{F}} \cdot \hat{\mathbf{i}}'' \end{cases} \tag{26}$$

By controlling the relative position between the coils and the microrobot, i.e, $\mathbf{p}_{\mathrm{PW}}^{\mathcal{G}}$, we ensure $\tilde{\mathbf{f}}'$ and $\tilde{\mathbf{f}}''$ are linearly independent and utilize the two force DoFs to actuate the 3D motion of microrobots. Firstly, considering the gravity force, we ensure the magnetic force in the $z^{\mathcal{G}}$ direction equals the desired one, i.e., $\mathbf{f}_{\mathrm{d}}.z$, by

$$\tilde{\mathbf{f}}'.z \cdot I_1 + \tilde{\mathbf{f}}''.z \cdot I_2 = \mathbf{f}_{\mathrm{d}}.z \tag{27}$$

where I_1 and I_2 are coefficients to be solved. The second condition to fulfill is that the direction of the magnetic force in the xy plane equals the desired one:

$$\begin{cases} \frac{\tilde{\mathbf{f}}'.y \cdot I_1 + \tilde{\mathbf{f}}''.y \cdot I_2}{\tilde{\mathbf{f}}'.x \cdot I_1 + \tilde{\mathbf{f}}''.x \cdot I_2} = \frac{\mathbf{f}_{\mathrm{d}}.y}{\mathbf{f}_{\mathrm{d}}.x}, \text{ if } \mathbf{f}_{\mathrm{d}}.x \neq 0 \\ \tilde{\mathbf{f}}'.x \cdot I_1 + \tilde{\mathbf{f}}''.x \cdot I_2 = 0, \text{ if } \mathbf{f}_{\mathrm{d}}.x = 0 \end{cases} \tag{28}$$

Now, combining Eqs. (27) and (28), we can obtain I_1 and I_2, and the final coil current vector $\mathbf{i}$ is

$$\mathbf{i} = \hat{\mathbf{i}}' \cdot I_1 + \hat{\mathbf{i}}'' \cdot I_2 \tag{29}$$

and the resulting magnetic force is $\mathbf{f} = \bar{\mathbf{F}} \cdot \mathbf{i}$. In order to make sure Eqs. (27)(28) have feasible $\mathbf{i}$ and also to optimize $\mathbf{i}$, we adjust the xy component of $\mathbf{p}_{\mathrm{PW}}^{\mathcal{G}}$, i.e., $\mathbf{p}_{\mathrm{PW}}^{\mathcal{G}}.xy$ to minimize the following cost function:

$$Cost = W_1 \cdot ||\hat{\mathbf{f}}.xy - \hat{\mathbf{f}}_{\mathrm{d}}.xy|| - W_2 \cdot ||\mathbf{f}.xy|| + ||\mathbf{i}|| \tag{30}$$

Where W_1 and W_2 are constant weights, and the three terms are to minimize the force direction error in the xy plane, maximize the resulting magnetic force in the xy plane, and minimize the coil currents, respectively. By this optimization process, the coil positions and coil currents could be obtained to generate the desired robot orientation and motion.

V. Validation Results

A. Control of the Over-Constrained Parallel Mechanism

We first conduct experiments to validate if the mechanical motion of the constructed QuadMag can be well controlled by our control method. We implement the method presented in Section III on the Arduino with a control frequency of 100 Hz, i.e., $\Delta t = 0.01$ s. During the validation, after initializing the position of the coil-end plate ($\mathbf{p}_{\mathrm{P}}^{\mathcal{G}}$) to $[0\ 0\ 30]^{\mathrm{T}}$, we sequentially input five positions to let the coil-end plate to reach, which are $[100\ 0\ 60]^{\mathrm{T}}$, $[0\ -100\ 60]^{\mathrm{T}}$, $[-100\ 0\ 30]^{\mathrm{T}}$, $[100\ 0\ 30]^{\mathrm{T}}$, and $[0\ 0\ 30]^{\mathrm{T}}$. The desired motion speed is set as 5 mm/s. As shown in Fig. 3 and the Supporting video, the over-constrained parallel mechanism reaches all the commanded positions without instability, proving the correctness of the proposed differential control method and validating the applicability of the constructed system.

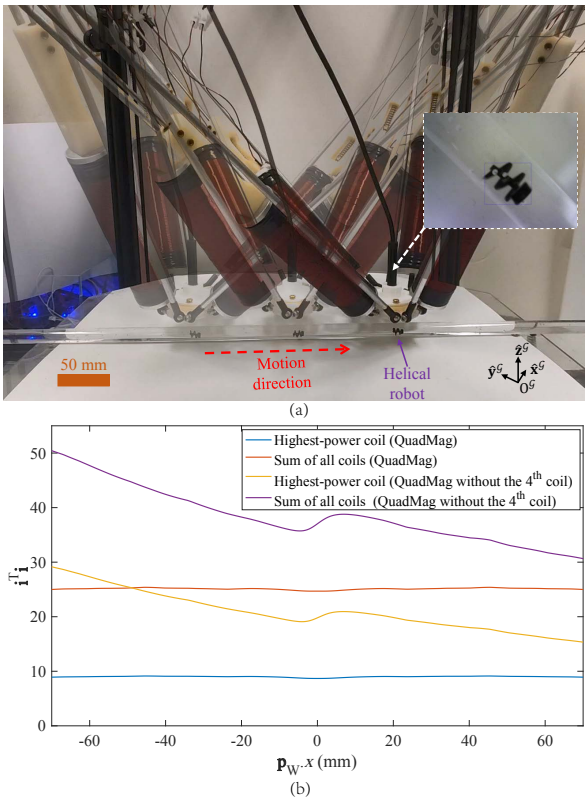

Fig. 4. Actuation of a magnetic helical robot ($\Phi 5 \times 10$ mm) swimming through a lumen filled with water. (a) The experiment process that the robot moves from $[-70\ -70\ 0]^{\mathrm{T}}$ to $[70\ 70\ 0]^{\mathrm{T}}$. The inset shows the feedback image from the camera. (b) The power consumed by the QuadMag and QuadMag without the 4^{th} coil during actuation experiments.

B. Enhanced Actuation Efficiency

To quantitatively validate the actuation efficiency of QuadMag, we perform experiments to actuate a helical robot swimming through a lumen. For comparison, we repeat the experiment using three coils, i.e., QuadMag without the 4^{th} coil. As shown in Fig. 4(a) and the Supporting video, driven by the generated rotating fields, the magnetic helical robot ($\Phi 5 \times 10$ mm) swims from $[-70\ -70\ 0]^{\mathrm{T}}$ to $[70\ 70\ 0]^{\mathrm{T}}$. The magnetic fields are computed by the method described in Section IV. A with frequency and strength of 4 Hz and 3 mT, respectively. $\mathbf{p}_{\mathrm{PW}}^{\mathcal{G}}$ is set as $[0\ 0\ -35]^{\mathrm{T}}$. Experiments validate the correctness of the field generation method, and Fig. 4(b) plots the consumed power ($\mathbf{i}^{\mathrm{T}}\mathbf{i}$) during the experiments.

Results show that, the total power of all the coils of QuadMag is always less than that when using three coils, and the total power for this task is reduced by 37.7%, reflecting the enhanced actuation efficiency. When using four coils, the electric current of the highest-power coil is also dramatically reduced that lowers the requirement on the servo-amplifier.

C. Simulated 3D Force-Driven Navigation With Controlled Robot Orientation

We validate the simultaneous field and force control capability of QuadMag by actuating a force-driven microrobot to follow a 3D path with controlled robot orientation. The robot moves in free fluid, and its net gravity force and magnetic moment are set as $F_g = 0.522$ mN and $||\mathbf{m}^{\mathcal{G}}|| = 0.0102$ A·m^2, respectively. As shown in Fig. 5, the desired 3D circular path has a radius of 60 mm and is composed of 50 waypoints. The microrobot starts from $\mathbf{p}_{\mathrm{s}}^{\mathcal{G}} = [0\ 0\ \text{-}50]^{\mathrm{T}}$, whose desired magnetic force is calculated by

$$\mathbf{f}_{\mathrm{d}} = W_{\mathrm{c}} \cdot (\mathbf{p}_{\mathrm{d}j}^{\mathcal{G}} - \mathbf{p}_{\mathrm{W}}^{\mathcal{G}}) + [0\ 0\ F_g]^{\mathrm{T}} \tag{31}$$

where $\mathbf{p}_{\mathrm{d}j}^{\mathcal{G}}$ is the j-th desired waypoint, which is updated to $\mathbf{p}_{\mathrm{d}j+1}^{\mathcal{G}}$ when the robot reaches $\mathbf{p}_{\mathrm{d}j}^{\mathcal{G}}$ within a distance threshold $\delta = 2$ mm. The control gain W_{c} is set as 0.00005, and then the obtained desired force is used to compute the coil currents and the resulting force $\mathbf{f}$ via the method in Section IV. C where W_1 and W_2 are set as 1000 and 1, respectively. Assuming a low-Reynolds-number condition, the robot position at the next control interval is

$$\mathbf{p}_{\mathrm{W}+}^{\mathcal{G}} = \mathbf{p}_{\mathrm{W}}^{\mathcal{G}} + t_{\mathrm{c}} \cdot \frac{\mathbf{f} - [0\ 0\ F_g]^{\mathrm{T}}}{6\pi\mu R} \tag{32}$$

where $t_{\mathrm{c}} = 0.2$ s, $\mu = 81.5$ mPa·s, and $R = 5$ mm are the control interval, fluid viscosity, and equivalent robot radius, respectively. Repeating the above calculation process, the robot navigation trajectory can be obtained.

1) Task #1: robot orientation perpendicular to path: We assume the robot orientation refers to the magnetic moment direction. Regarding this task, the robot orientation is required to point to the center of a 3D circular path (diameter: 120 mm) as shown in Fig. 5(a). Results in the Supporting video show that the orientation of the robot fulfill the requirement, and the robot successfully navigates along the 3D path trajectory with a maximum error < 5 mm, validating the capability of the QuadMag system for simultaneous field and force control.

2) Task #2: robot orientation parallel to path: For this task, the robot orientation is required to be parallel to the path, and the navigation results are illustrated in Fig. 5(b) and the Supporting video, which also validate the enhanced actuation dexterity for different orientation requirements. Fig. 5(c) plots the variations of the $\mathbf{p}_{\mathrm{PW}}^{\mathcal{G}}.xy$, which is selected from 20 candidates ($30 \times [\cos(18j)\ \sin(18j)]^{\mathrm{T}}\ j = 0, 1, \cdots, 19$) determined by the cost function in Eq. (30). It is noted that the coil-end plate may have sudden long-distance changes during the tasks, which could be avoided in the future by considering this factor in the cost function.

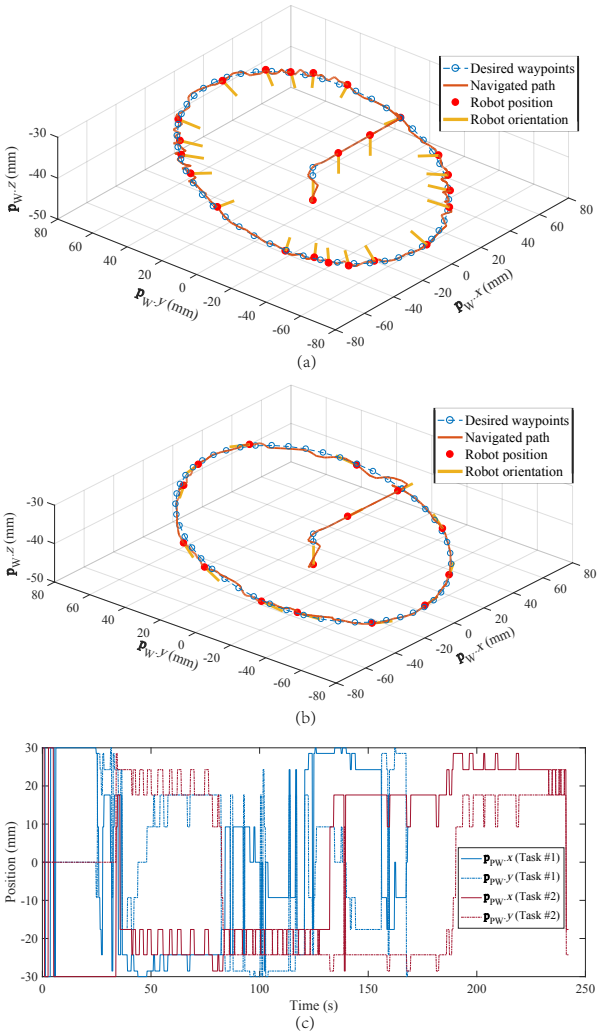

Fig. 5. Simulated 3D force-driven navigation results with controlled robot orientation. (a) The robot orientation is required to perpendicular to the navigation path. (b) The robot orientation is required to parallel to the navigation path. (c) Variations of $\mathbf{p}_{\mathrm{PW}}^{\mathcal{G}}.xy$ during the two tasks.

VI. Conclusion

In this paper, we have presented QuadMag–a magnetic actuation system with four mobile coils. To control the mechanical motion of the over-constrained parallel mechanism, we proposed a differential method and validated its feasibility via experiments. We also proposed the magnetic field, force, and simultaneous field and force control methods for QuadMag with validations via experiments and simulated navigation. Comparative results proved the enhanced efficiency of QuadMag when actuating a magnetic helical robot compared with DeltaMag. The actuation capability for 3D magnetic force-based navigation with different required robot orientation is also demonstrated.

In the future, experiments will be conducted to reproduce the simultaneous field and force control method after modification of the cost function and necessary control methods. Extra experiment scenarios would also be designed to show the manipulation capabilities of QuadMag.

REFERENCES

[1] B. J. Nelson, I. K. Kaliakatsos, and J. J. Abbott, "Microrobots for minimally invasive medicine," *Ann. Rev. Biomed. Eng.*, vol. 12, pp. 55–85, 2010.

[2] M. Sitti, H. Ceylan, W. Hu, J. Giltinan, M. Turan, S. Yim, and E. Diller, "Biomedical applications of untethered mobile milli/microrobots," *Proc. IEEE*, vol. 103, no. 2, pp. 205–224, 2015.

[3] T.-Y. Huang, H. Gu, and B. J. Nelson, "Increasingly intelligent micromachines," *Ann. Rev. Control Robot. Auton. Syst.*, vol. 5, pp. 279–310, 2022.

[4] L. Yang, J. Yu, S. Yang, B. Wang, B. J. Nelson, and L. Zhang, "A survey on swarm microrobotics," *IEEE Trans. Robot.*, vol. 38, no. 3, pp. 1531–1551, 2022.

[5] O. Felfoul, M. Mohammadi, S. Taherkhani, D. De Lanauze, Y. Zhong Xu, D. Loghin, S. Essa, S. Jancik, D. Houle, M. Lafleur, *et al.*, "Magneto-aerotactic bacteria deliver drug-containing nanoliposomes to tumour hypoxic regions," *Nat. Nanotechnol.*, vol. 11, no. 11, pp. 941–947, 2016.

[6] J. Li, X. Li, T. Luo, R. Wang, C. Liu, S. Chen, D. Li, J. Yue, S.-h. Cheng, and D. Sun, "Development of a magnetic microrobot for carrying and delivering targeted cells," *Sci. Robot.*, vol. 3, no. 19, 2018.

[7] X. Wang, C. Ho, Y. Tsatskis, J. Law, Z. Zhang, M. Zhu, C. Dai, F. Wang, M. Tan, S. Hopyan, *et al.*, "Intracellular manipulation and measurement with multipole magnetic tweezers," *Sci. Robot.*, vol. 4, no. 28, p. eaav6180, 2019.

[8] B. Wang, K. F. Chan, K. Yuan, Q. Wang, X. Xia, L. Yang, H. Ko, Y.-X. J. Wang, J. J. Y. Sung, P. W. Y. Chiu, *et al.*, "Endoscopy-assisted magnetic navigation of biohybrid soft microrobots with rapid endoluminal delivery and imaging," *Sci. Robot.*, vol. 6, no. 52, p. eabd2813, 2021.

[9] J. Law, X. Wang, M. Luo, L. Xin, X. Du, W. Dou, T. Wang, G. Shan, Y. Wang, P. Song, *et al.*, "Microrobotic swarms for selective embolization," *Sci. Adv.*, vol. 8, no. 29, p. eabm5752, 2022.

[10] P. E. Dupont, B. J. Nelson, M. Goldfarb, B. Hannaford, A. Menciassi, M. K. OâMalley, N. Simaan, P. Valdastri, and G.-Z. Yang, "A decade retrospective of medical robotics research from 2010 to 2020," *Sci. Robot.*, vol. 6, no. 60, p. eabi8017, 2021.

[11] J. C. Norton, P. R. Slawinski, H. S. Lay, J. W. Martin, B. F. Cox, G. Cummins, M. P. Desmulliez, R. E. Clutton, K. L. Obstein, S. Cochran, *et al.*, "Intelligent magnetic manipulation for gastrointestinal ultrasound," *Sci. Robot.*, vol. 4, no. 31, p. eaav7725, 2019.

[12] Y. Kim, E. Genevriere, P. Harker, J. Choe, M. Balicki, R. W. Regenhardt, J. E. Vranic, A. A. Dmytriw, A. B. Patel, and X. Zhao, "Telerobotic neurovascular interventions with magnetic manipulation," *Sci. Robot.*, vol. 7, no. 65, p. eabg9907, 2022.

[13] L. Yang and L. Zhang, "Motion control in magnetic microrobotics: From individual and multiple robots to swarms," *Annu. Rev. Control Robot. Auton. Syst.*, vol. 4, pp. 509–534, 2021.

[14] L. Arcese, M. Fruchard, and A. Ferreira, "Adaptive controller and observer for a magnetic microrobot," *IEEE Trans. Robot.*, vol. 29, no. 4, pp. 1060–1067, 2013.

[15] E. Diller, J. Giltinan, and M. Sitti, "Independent control of multiple magnetic microrobots in three dimensions," *Int. J. Robot. Res.*, vol. 32, no. 5, pp. 614–631, 2013.

[16] T. Xu, C. Huang, Z. Lai, and X. Wu, "Independent control strategy of multiple magnetic flexible millirobots for position control and path following," *IEEE Trans. Robot.*, 2022.

[17] H. Xie, M. Sun, X. Fan, Z. Lin, W. Chen, L. Wang, L. Dong, and Q. He, "Reconfigurable magnetic microrobot swarm: Multimode transformation, locomotion, and manipulation," *Sci. Robot.*, vol. 4, no. 28, p. eaav8006, 2019.

[18] J. Yu, L. Yang, and L. Zhang, "Pattern generation and motion control of a vortex-like paramagnetic nanoparticle swarm," *Int. J. Robot. Res.*, vol. 37, no. 8, pp. 912–930, 2018.

[19] X. Dong and M. Sitti, "Controlling two-dimensional collective formation and cooperative behavior of magnetic microrobot swarms," *The Int. J. Robot. Res.*, vol. 39, no. 5, pp. 617–638, 2020.

[20] L. Yang, J. Jiang, X. Gao, Q. Wang, Q. Dou, and L. Zhang, "Autonomous environment-adaptive microrobot swarm navigation enabled by deep learning-based real-time distribution planning," *Nat. Mach. Intell.*, vol. 4, no. 5, pp. 480–493, 2022.

[21] J. J. Abbott, E. Diller, and A. J. Petruska, "Magnetic methods in robotics," *Annu. Rev. Control Robot. Auton. Syst.*, vol. 3, pp. 57–90, 2020.

[22] A. W. Mahoney and J. J. Abbott, "Five-degree-of-freedom manipulation of an untethered magnetic device in fluid using a single permanent magnet with application in stomach capsule endoscopy," *Int. J. Robot. Res.*, vol. 35, no. 1-3, pp. 129–147, 2016.

[23] P. Ryan and E. Diller, "Magnetic actuation for full dexterity microrobotic control using rotating permanent magnets," *IEEE Trans. Robot.*, vol. 33, no. 6, pp. 1398–1409, 2017.

[24] J. W. Martin, B. Scaglioni, J. C. Norton, V. Subramanian, A. Arezzo, K. L. Obstein, and P. Valdastri, "Enabling the future of colonoscopy with intelligent and autonomous magnetic manipulation," *Nat. Mach. Intell.*, vol. 2, no. 10, pp. 595–606, 2020.

[25] A. Oulmas *et al.*, "3d closed-loop swimming at low reynolds numbers," *Int. J. Robot. Res.*, vol. 37, no. 11, pp. 1359–1375, 2018.

[26] M. Kummer *et al.*, "Octomag: An electromagnetic system for 5-dof wireless micromanipulation," *IEEE Trans. Robot.*, vol. 26, no. 6, pp. 1006–1017, 2010.

[27] I. S. Khalil *et al.*, "Closed-loop control of magnetotactic bacteria," *Int. J. Robot. Res.*, vol. 32, no. 6, pp. 637–649, 2013.

[28] H. Choi, K. Cha, S. Jeong, J.-o. Park, and S. Park, "3-d locomotive and drilling microrobot using novel stationary ema system," *IEEE/ASME Trans. Mechatron.*, vol. 18, no. 3, pp. 1221–1225, 2012.

[29] J. Edelmann, A. J. Petruska, and B. J. Nelson, "Magnetic control of continuum devices," *Int. J. Robot. Res.*, vol. 36, no. 1, pp. 68–85, 2017.

[30] C. Chautems and B. J. Nelson, "The tethered magnet: Force and 5-dof pose control for cardiac ablation," in *Robot. Autom. (ICRA), 2017 IEEE Int. Conf.* IEEE, 2017, pp. 4837–4842.

[31] B. Veron *et al.*, "Geometric analysis of the singularities of a magnetic manipulation system with several mobile coils," in *Intell. Robot. Syst. (IROS), 2013 IEEE/RSJ Int. Conf.* IEEE, 2013, pp. 4996–5001.

[32] J. Sikorski, C. M. Heunis, F. Franco, and S. Misra, "The armm system: An optimized mobile electromagnetic coil for non-linear actuation of flexible surgical instruments," *IEEE trans. Magnetics*, vol. 55, no. 9, pp. 1–9, 2019.

[33] L. Yang, X. Du, E. Yu, D. Jin, and L. Zhang, "Deltamag: An electromagnetic manipulation system with parallel mobile coils," in *2019 Int. Conf. Robot. Autom. (ICRA)*. IEEE, 2019, pp. 9814–9820.

[34] X. Du, M. Zhang, J. Yu, L. Yang, P. W. Y. Chiu, and L. Zhang, "Design and real-time optimization for a magnetic actuation system with enhanced flexibility," *IEEE/ASME Trans. Mechatron.*, vol. 26, no. 3, pp. 1524–1535, 2020.

[35] Z. Yang, L. Yang, M. Zhang, C. Zhang, S. C. H. Yu, and L. Zhang, "Ultrasound-guided catheterization using a driller-tipped guidewire with combined magnetic navigation and drilling motion," *IEEE/ASME Transactions on Mechatronics*, 2021.

[36] Z. Yang, L. Yang, and L. Zhang, "Autonomous navigation of magnetic microrobots in a large workspace using mobile-coil system," *IEEE/ASME Trans. Mechatron.*, vol. 26, no. 6, pp. 3163–3174, 2021.

[37] A. J. Petruska and B. J. Nelson, "Minimum bounds on the number of electromagnets required for remote magnetic manipulation," *IEEE Trans. Robot.*, vol. 31, no. 3, pp. 714–722, 2015.